Iraqi journal of Bioscience and Biomedical
Published Online First: 31/December/ /2025.
p-ISSN: 3007-5491 / e-ISSN:3007-5505

A Novel Sphingosomes Nanocarrier for β-Elemonic Acid Delivery

***Sarah Sabri*[1*] *Noora A. Hadi*[2]**

[1] Department of plant Biotechnology, Collage of Biotechnology, Al-Nahrain University, Baghdad, Iraq.
[2] Department of plant Biotechnology, Collage of Biotechnology, Al-Nahrain University, Baghdad, Iraq

*Corresponding author: sarah1995adil@gmail.com

Received: **2025/11/16, Accepted**: **2025/12/21, Published: 2025/12/31** .

Abstract

Nanotechnology-based drug delivery systems have gained increasing attention as effective strategies to enhance therapeutic efficiency while reducing systemic toxicity. In this study, β-elemonic acid was extracted from *Boswellia carterii* resin utilized High-performance liquid chromatography analysis and identified as a natural triterpenoid based on its structural characteristics. Sphingosomes nanoparticles were subsequently prepared using the methanol injection method. The prepared sphingosomes were characterized using Field Emission Scanning Electron Microscopy (FESEM) and Atomic Force Microscopy (AFM). FESEM analysis revealed spherical and uniformly distributed nanoparticles within the nanoscale range without noticeable aggregation. AFM results further confirmed the nanoscale dimensions, showing consistent particle height and diameter with low surface roughness. Fourier Transform Infrared Spectroscopy (FTIR) was employed to characterize β-elemonic acid, revealing distinct functional groups. After incorporation into the sphingosomes formulation, slight shifts in characteristic band were observed, indicating molecular interactions and successful encapsulation within the lipid matrix. These findings demonstrate the effective extraction, formulation, and physicochemical characterization of a lipid-based nanocarrier system with potential relevance for drug delivery applications.

Keywords: Sphingosomes nanparticles, active compound encapsulation.

Introduction

Bio-fabrication involves the development of biologically functional products through the use of living cells, biomolecules, and other bio-derived materials [1]. In recent years, advances in nanotechnology have provided effective approaches to address several limitations of conventional chemotherapy, offering improved strategies for cancer treatment [2]. In this context, nanoparticle-based drug delivery systems have attracted considerable attention due to their ability to enhance in tumor accumulation and retention through the enhanced permeability and retention (EPR) effect, while reducing the adverse effects associated with

Iraqi journal of Bioscience and Biomedical
Published Online First: 31/December/ /2025.
p-ISSN: 3007-5491 / e-ISSN:3007-5505

traditional cancer therapies [3]. Furthermore, nanocarriers contribute to prolonged drug half-life, enable controlled release profiles, and facilitate site-specific delivery of therapeutic agents [4].

Sphingosomes (Sph) are lipid-based nanocarrier overcome limitations of vesicle systems, including instability, short systemic circulation time, and limited accumulation in tumor tissue [5]. The main advantages of Sph lie in their capacity to passively accumulate in tumor tissues, which enhances therapeutic efficacy and allows for controlled drug release. Moreover, they improve drug stability, reduce systemic toxicity, and exhibit favorable pharmacokinetic behavior by prolonging the circulation time of therapeutic agents in the body. In addition, the incorporation of sphingolipids into nanocarrier systems supports active targeting strategies through the attachment of site-specific ligands, thereby increasing treatment specificity and overall effectiveness [18]. Sph have been investigated as potential drug delivery systems in various cancers type, such as colonic tumors, breast cancer, non-small cell lung cancer, melanoma, ovarian cancer, and lymphomas, where lipid-based formulations improved the therapeutic index and overall efficacy of conventional anticancer agent [6].

Recently, natural products have gained growing interest as potential anticancer agents because of their accessibility, biocompatibility, and relatively low toxicity [7]. Plant-derived compounds have been widely investigated due to their long history of use in traditional medicine and their demonstrated biological activity against various diseases .[8].

Boswellia Carterii (B.Carterii) resin is a source of multiple bioactive compounds, including flavonoids, isoflavones, terpenoids, polyphenols, tannins, etc. [9]. Triterpenic acids have received particular attention due to their selective cytotoxic effects against cancer cells while showing minimal toxicity toward normal cells [10]. β-Elemonic acid (β-EA), has been reported to possess favorable physicochemical properties, such as relatively low molecular weight and high lipid solubility, which may facilitate its transport across biological barriers. Previous studies have shown that β-EA exhibits anticancer activity by promoting cancer cell death and suppressing of key pathways involved in tumor growth [11,12]. Moreover, β-EA has been found to inhibit the cell cycle at modest concentrations and induces apoptosis in cancer cells [19,20].

Isolation and Identification of β-EA by High-performance liquid chromatography (HPLC).

HPLC was employed in this study due to its well-established reliability in the isolation and quantification of triterpenic acids and terpenoids derived from *Boswellia* species. While previous studies have primarily focused on the analysis of boswellic acids, such as acetyl-11-keto-β-boswellic acid (AKBA) and keto-β-boswellic acid (KBA), limited information is available regarding the HPLC-based detection of β-elemonic acid. Therefore, HPLC analysis was utilized to support the identification of β-EA in this study [13].

The HPLC analysis of the standard β-EA displayed a single sharp peak at 5.72 min (Figure 1-1a), confirming its purity. In comparison, the *B.Carterii* resin extract presented several peaks, among which a dominant one was observed at 5.71 min (Figure 1-1b).

Iraqi journal of Bioscience and Biomedical
Published Online First: 31/December/ /2025.
p-ISSN: 3007-5491 / e-ISSN:3007-5505

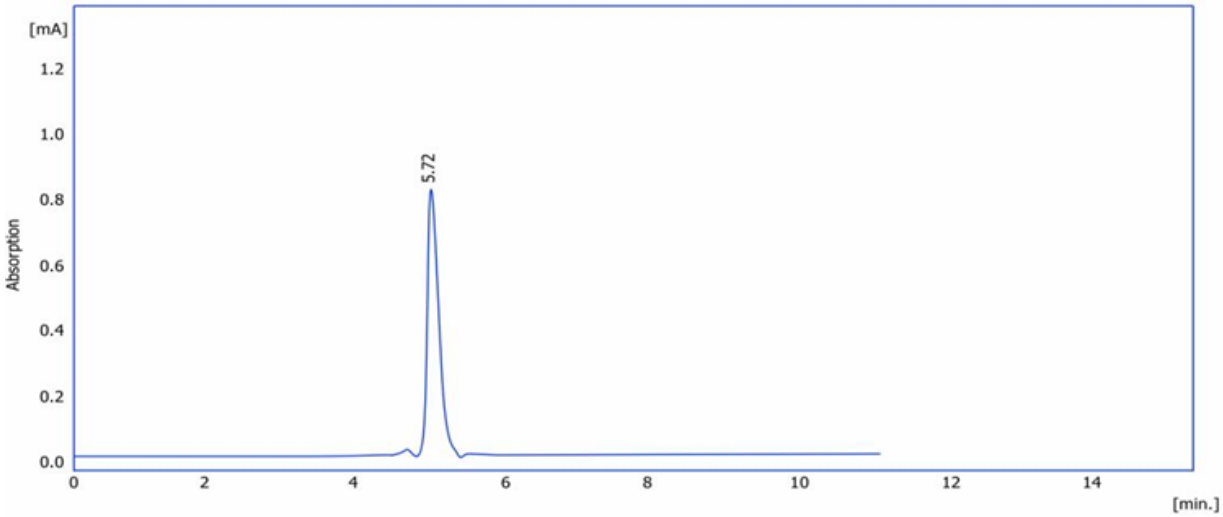

Result chromatography Table (Uncal - F:\ B-elemonic acid 2 ppm)

No	Reten. Time [min]	Area [mAU.s]	Height [mAU]	Area [%]	Height [%]	W05 [min]	Compound Name
1	5.72	798.08	801.44	100.00	100.00	0.08	
	Total	798.08	801.44	100.00	100.00		

Figure 1-1: a. HPLC chromatography and corresponding peak table of stander β-EA.

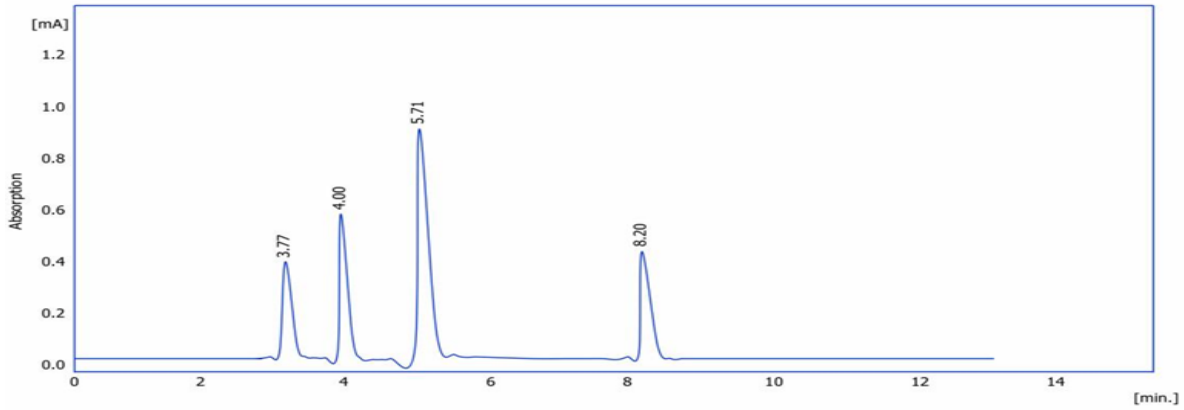

Result chromatography Table (Uncal - F:\ gum)

No	Reten. Time [min]	Area [mAU.s]	Height [mAU]	Area [%]	Height [%]	W05 [min]	Compound Name
1	3.77	9855.08	386.98	15.00	15.00	0.05	
2	4.00	16524.59	544.70	20.00	20.00	0.07	
3	5.71	88952.25	830.65	50.00	50.00	0.15	
4	8.20	8541.23	420.33	15.00	15.00	0.05	
	Total	123784.09	2182.56	100.00	100.00		

Figure 1-1: b. HPLC chromatography and corresponding peak table of *B.Carterii* extract show mutable peaks. Refer in figure *B.Carterii* as (gum).

Iraqi journal of Bioscience and Biomedical
Published Online First: 31/December/ /2025.
p-ISSN: 3007-5491 / e-ISSN:3007-5505

Preparation of Sphingosomes nanocarrier

Initially, the β-EA was obtained as a pure white crystalline powder. Upon the addition of the prepared Sph NPs" which initially had a pale-yellow tint "the suspension gradually shifted to a brownish colour. This gradual colour change served as clear evidence that the β-EA had been successfully incorporated loaded into the nanocarrier. (Figure 1-2).

Figure 1-2: Formation of β-EA loaded Sphingosomes nanocarrier.

Atomic Force Microscopy (AFM)

Atomic Force Microscopy (AFM) was utilized to obtain topographical information and confirm the nanoscale morphology of the sample. A two-dimensional (2D) AFM image was first acquired over a scan area of 1.25 μm × 1.25 μm, which revealed the lateral distribution of the Sph nanocarrier (Figure 2a). From this image, the average particle diameter was estimated to be approximately ≈ 83.5 nm, and the surface morphology showed a moderately rough surface profile, as summarized in (Table 1) [14]. The corresponding three-dimensional (3D) AFM image provided information on the vertical dimension (Z-axis), where the maximum peak height reached about +4.58 nm and the lowest point was around –2.17 nm, resulting in a total height difference of nearly 6.75 nm. Thus, their vertical height did not exceed 5–7 nm.

The AFM histogram shows the granularity distribution of Sph nanocarrier, where most particles were in the range of 60-120 nm with an average around 80-90 nm (Figure 2b). This indicates a relatively uniform nanoscale distribution, supporting the stability of the carrier system. These findings are in consistent with previously reported data, where lipid-based nanocarriers used for drug delivery typically exhibit particle sizes in the range of 10-150 nm [15].

Iraqi journal of Bioscience and Biomedical
Published Online First: 31/December/ /2025.
p-ISSN: 3007-5491 / e-ISSN:3007-5505

Table 1: average diameter and height distribution of β-EA loaded Sph nanocarrier.

	Average Diameter	height distribution
β-EA loaded Sph nanocarrier	≈ 83.5 nm	≈ 6.75 nm

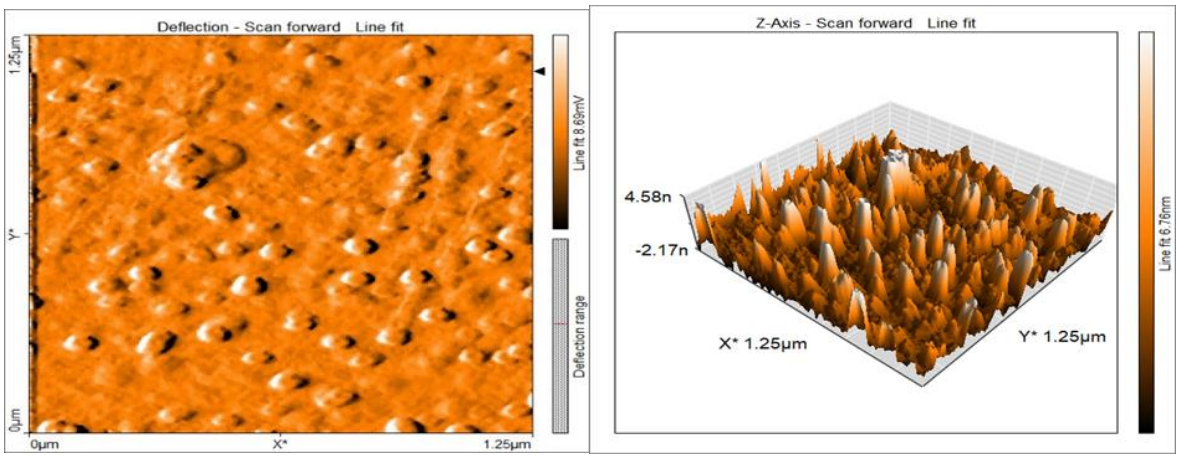

Figure 2: a. AFM 2/3-dimensional image of sphingosomes nanocarrier.

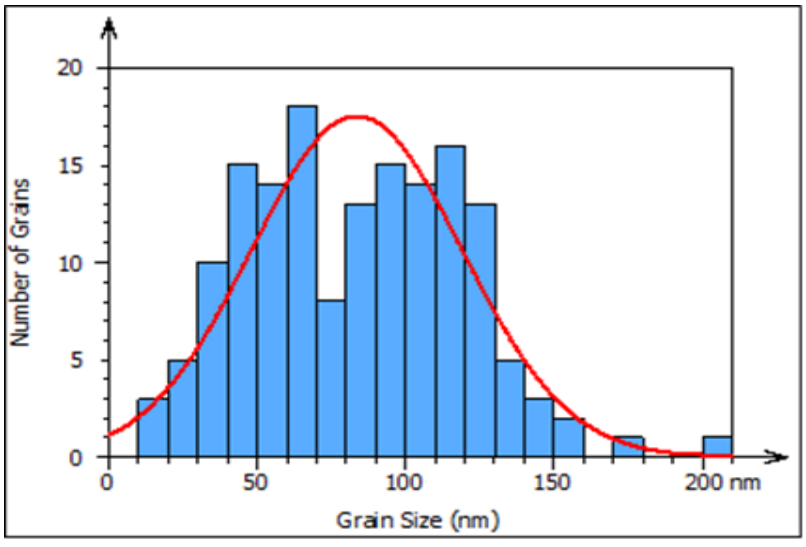

Figure 2: b. Result of AFM histogram showing granularity distribution of Sph nanocarrier.

Iraqi journal of Bioscience and Biomedical
Published Online First: 31/December/ /2025.
p-ISSN: 3007-5491 / e-ISSN:3007-5505

Field Emission Scanning Electron Microscopy (FESEM)

The morphological characteristics of β-EA loaded Sph nanocarrier were examined using field emission scanning electron microscopy (FESEM). At a magnification of 30,000× (scale bar = 3 μm), the FESEM micrographs (Figure 3a) illustrated the overall distribution of the Sph nanocarriers, showing a homogeneous dispersion across the surface with no obvious signs of particle aggregation. Higher magnification images obtained at 120,000× (scale bar = 500 nm) enabled clearer visualization of the nanocarriers morphology. The Sph nanocarrier predominantly exhibited a spherical shape with relatively smooth surface features. Particle size analysis revealed diameters ranging from 28.6 to 52.4 nm, with an average particle size of approximately 40 nm, confirming their nanoscale dimensions (Figure 3b). These findings indicate that the prepared nanoparticles possess uniform morphology and favorable surface characteristics, which are essential for improving stability, enhancing cellular uptake, and supporting effective targeted drug delivery [16].

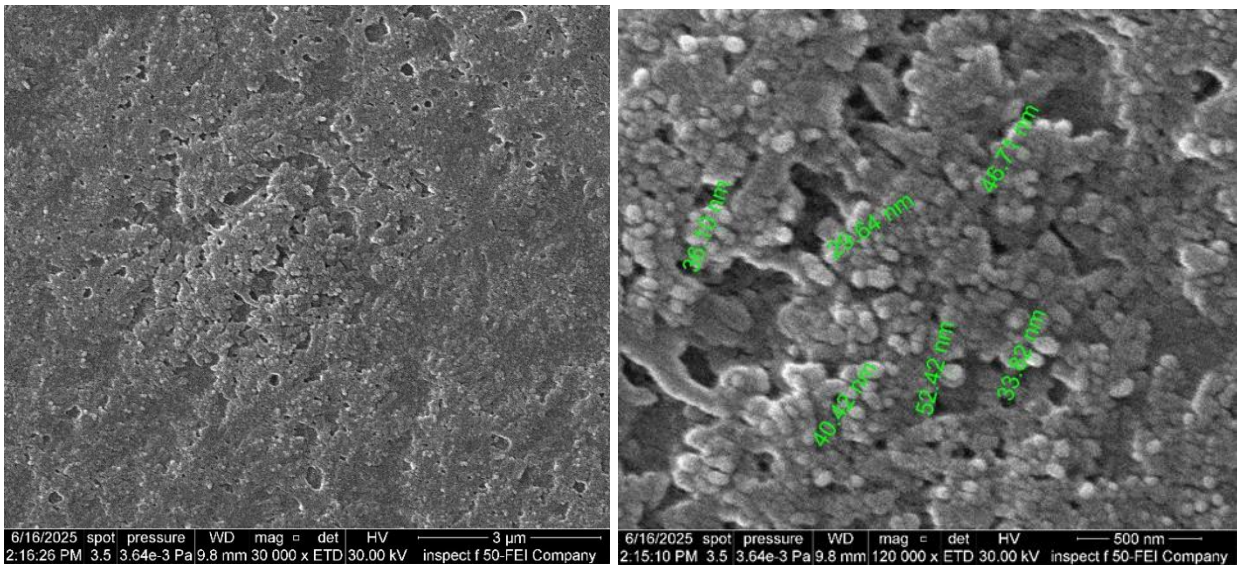

a. **b.**

Figure 3: FESEM image of Sph nanocarrier morphology a. magnificent 30k and b. magnificent 120k.

Iraqi journal of Bioscience and Biomedical
Published Online First: 31/December/ /2025.
p-ISSN: 3007-5491 / e-ISSN:3007-5505

Fourier Transform Infrared Spectroscopy Analysis (FT-IR)

For this study, The FTIR spectrum was interpreted according to standard infrared absorption frequency reference [17]. A band was observed at approximately 3431 cm^{-1} (Figure 4b), this region can primarily be assigned to O–H and N–H stretching vibrations, suggesting the presence of hydrogen bonding interactions between the hydroxyl and amide groups of Sph and the carboxylic and hydroxyl groups of β-EA. Additionally, also may correspond to =C–H stretching of unsaturated triterpenoid rings originating from β-EA, which is consistent with its chemical structure containing conjugated double bonds. The shift from 2362 in β-EA spectrum (Figure 4a) to 2366 cm^{-1} and the appearance of a new band at 2310 cm^{-1} indicate a molecular interaction between β-EA and the Sph nanocarrier. The disappearance of the band at 1705 cm^{-1} (Figure 4b), indicates a possible interaction and bonding between the active compound and the nanocarrier.

Moreover, the characteristic stretching band of β-EA at around 1654 cm^{-1} shifted to the range of approximately 1643–1633 cm^{-1} after encapsulation into Sph nanocarrier. This shift indicates an interaction between the carbonyl group of β-EA and the polar head groups of the nanocarrier, most likely through hydrogen bonding with amide N–H or C=C alkenes. Such shifts are commonly observed when a drug is successfully incorporated into a phospholipid-based nanocarrier, confirming the effective encapsulation of β-EA into Sph system. In addition (Figure 4a), the disappearance of the band at 1375 cm^{-1} and the shift of the band from 1458 cm^{-1} to 1409 cm^{-1} after encapsulation (Figure 4b), suggest interactions between aliphatic C=C stretching vibration of aromatic ring of β-EA and the carbon chains of the Sph. These changes indicate molecular interactions between the active compound and the nanocarrier. Furthermore, several characteristic bands of β-EA at 1286, 1197, 1112, and 1001 cm^{-1} disappeared after encapsulation. Meanwhile, a new band at 1134 cm^{-1} appeared in (Figure 4b), which may be attributed to C–O (alcohol), C–O–P (phpsphdioxy group), and C–N (aliphatic amine) stretching vibrations. This observation suggests the involvement of hydroxyl and phosphodiester groups in the interaction between β-EA and Sph NPs.

The disappearance of the 894 cm^{-1} band (Figure 4a) accompanied by the appearance of a new absorption at 950 cm^{-1} (Figure 4b), this region refers to O–H bending of the carboxylic acid group and =C–H bending of the alkenes compound. The band observed at 734 cm^{-1} (Figure 4b) shifting to 765 cm^{-1} refer to C–H out of plan bending vibration or/and N–H wagging from the sphingosomes matrix, indicating intermolecular interactions between β-EA and the amine groups. Disappeared of 663, 582 and 433 cm-1 band (Figure 4a) and appearance a band at 621 cm^{-1}, related to C–H bending, slightly shifted after β-EA interacted with the nanocarrier, indicating structural interaction between both components. All these spectral band changes together provide clear evidence of the interaction and successful encapsulation of β-EA within the Sph nanocarrier system.

Iraqi journal of Bioscience and Biomedical
Published Online First: 31/December/ /2025.
p-ISSN: 3007-5491 / e-ISSN:3007-5505

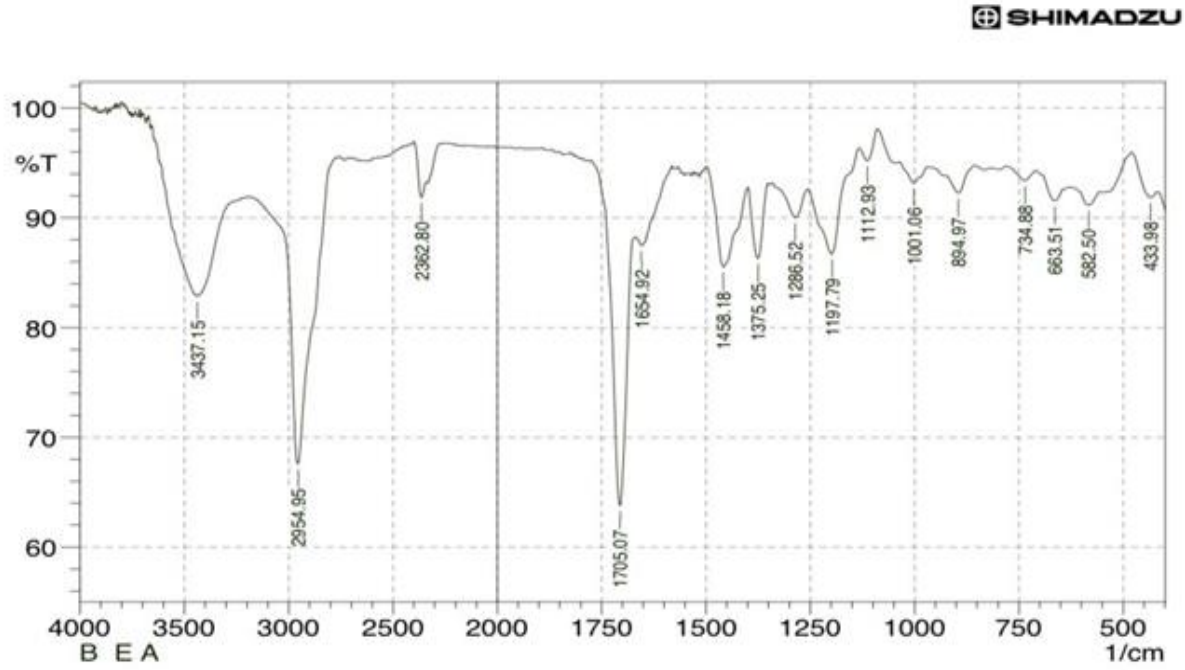

a.

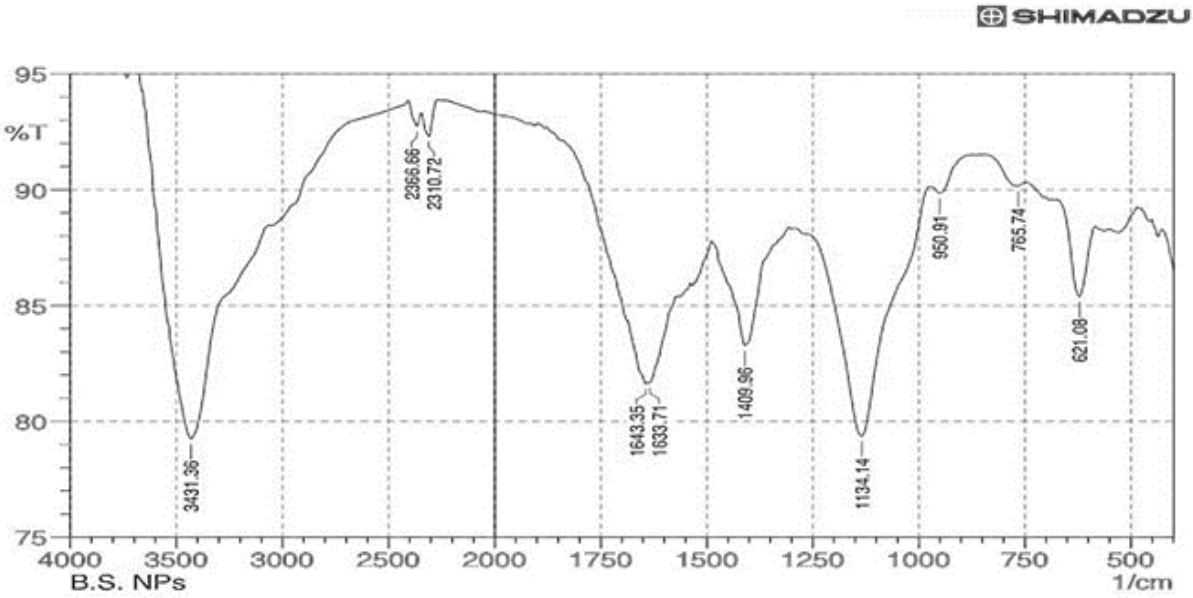

b.

Figure 4: FTIR spectrum of showing the characteristic absorption beak a. β-BA and b. β-EA loaded Sph nanocarrier.

Iraqi journal of Bioscience and Biomedical
Published Online First: 31/December/ /2025.
p-ISSN: 3007-5491 / e-ISSN:3007-5505

Conclusions

FTIR and FESEM analyses collectively confirmed the successful formation of β-EA–loaded Sph nanocarriers. The FTIR spectra showed characteristic shifts indicating molecular interactions between the β-EA and lipid matrix of Sph nanocarriers. FESEM images revealed well-defined, spherical nanoparticles with uniform morphology confirmed efficient encapsulation of the active compound.

Acknowledgments

Conduct further studies on *B.carterii* resin to isolate and identify the additional compounds observed during the HPLC analysis.

Author's Declaration

We hereby confirm that all tables and figures presented in this manuscript are original and were prepared by the authors. The study protocol was reviewed and approved by the Medical Ethics Committee of Al-Nahrain University/College of Biotechnology. All members provided informed assent after checking on the review depiction. The research was conducted in accordance with established ethical guidelines.

References

1. Wu, M., Ma, Z., Tian, Z., Rich, J. T., He, X., Xia, J., ... & Huang, T. J. (2024). Sound innovations for biofabrication and tissue engineering. Microsystems & Nanoengineering, 10(1), 170.
2. Giri, P. M., Banerjee, A., & Layek, B. (2023). A recent review on cancer nanomedicine. Cancers, 15(8), 2256.
3. Aboul-Nasr, M. B., Yasien, A. A., Mohamed, S. S., Aboul-Nasr, Y. B., & Obiedallah, M. (2025). Exploring the anticancer potential of green silver Nanoparticles–Paclitaxel nanocarrier on MCF-7 breast Cancer cells: an in vitro approach. Scientific Reports, 15(1), 20198.
4. Dabholkar, N., Waghule, T., Rapalli, V. K., Gorantla, S., Alexander, A., Saha, R. N., & Singhvi, G. (2021). Lipid shell lipid nanocapsules as smart generation lipid nanocarriers. Journal of Molecular Liquids, 339, 117145.
5. Konatham, T. K. R., & Alapati, S. (2023). A critical analysis of the vesicular drug delivery system: recent advancements and prospects for the future. Journal of innovations in applied pharmaceutical science (JIAPS), 5-12.
6. Shende, M., Ghode, P. D., Ghode, S., Bodele, S., Shende, A., & Nalawade, N. A. (2021). Sphingosomes: Highlights of the Progressive Journey and Their Application Perspectives in Modern Drug Delivery. World Journal of Pharmaceutical and Life Sciences, 7(10), 147–156.

Iraqi journal of Bioscience and Biomedical
Published Online First: 31/December/ /2025.
p-ISSN: 3007-5491 / e-ISSN:3007-5505

7. Rabiee, N., Ahmadi, S., Iravani, S., & Varma, R. S. (2023). Natural resources for sustainable synthesis of nanomaterials with anticancer applications: A move toward green nanomedicine. Environmental Research, 216, 114803.
8. Hashim, H. A., Mohammed, M. T., Thani, M. Z., & Klichkhanovb, N. K. (2024). Determination of Vitamins, Trace Elements, and Phytochemical Compounds in Boswellia Carterii Leaves Extracts.
9. Schmiech, M., Ulrich, J., Lang, S. J., Büchele, B., Paetz, C., St-Gelais, A., ... & Simmet, T. (2021). 11-Keto-α-boswellic acid, a novel triterpenoid from Boswellia spp. with chemotaxonomic potential and antitumor activity against triple-negative breast cancer cells. Molecules, 26(2), 366.
10. Hussain, H., Wang, D., El-Seedi, H. R., Rashan, L., Ahmed, I., Abbas, M., ... & Shah, S. T. A. (2024). Therapeutic potential of boswellic acids: an update patent review (2016–2023). Expert Opinion on Therapeutic Patents, 34(8), 723-732.
11. Xia, Y., Yang, J., Li, C., Hao, X., Fan, H., Zhao, Y., ... & Yang, J. (2022). TMT-based quantitative proteomics analysis reveals the panoramic pharmacological molecular mechanism of β-elemonic acid inhibition of colorectal cancer. Frontiers in Pharmacology, 13, 830328.
12. Bao, X., Zhu, J., Ren, C., Zhao, A., Zhang, M., Zhu, Z., ... & Ma, B. (2021). β-elemonic acid inhibits growth and triggers apoptosis in human castration-resistant prostate cancer cells through the suppression of JAK2/STAT3/MCL-1 and NF-κB signal pathways. Chemico-Biological Interactions, 342, 109477.
13. Asteggiano, A., Curatolo, L., Schiavo, V., Occhipinti, A., & Medana, C. (2023). Development, Validation, and Application of a Simple and Rugged HPLC Method for Boswellic Acids for a Comparative Study of Their Abundance in Different Species of Boswellia Gum Resins. Applied Sciences, 13(3), 1254. https://doi.org/10.3390/app13031254
14. Yilmaz, N., Yamada, T., Greimel, P., Uchihashi, T., Ando, T., & Kobayashi, T. (2013). Real-time visualization of assembling of a sphingomyelin-specific toxin on planar lipid membranes. Biophysical journal, 105(6), 1397-1405.
15. Xu, L., Wang, X., Liu, Y., Yang, G., Falconer, R. J., & Zhao, C. X. (2022). Lipid nanoparticles for drug delivery. Advanced NanoBiomed Research, 2(2), 2100109.
16. Al-Fatlawi, I.N.A.A., Pouresmaeil, V., Davoodi-Dehaghani, F. et al. Effects of solid lipid nanocarrier containing methyl urolithin A by coating folate-bound chitosan and evaluation of its anti-cancer activity. BMC Biotechnol 24, 18 (2024).
17. Silverstein, R. M., & Bassler, G. C. (1962). Spectrometric identification of organic compounds. Journal of Chemical Education, 39(11), 546.

18. Kumar, S., Singh, A., Pandey, P., Khopade, A., & Sawant, K. K. (2024). Application of sphingolipid-based nanocarriers in drug delivery: an overview. Therapeutic Delivery, 15(8), 619-637.
19. Xia, Y., Yang, J., Li, C., Hao, X., Fan, H., Zhao, Y., ... & Yang, J. (2022). TMT-based quantitative proteomics analysis reveals the panoramic pharmacological molecular mechanism of β-elemonic acid inhibition of colorectal cancer. Frontiers in Pharmacology, 13, 830328.
20. Wu, T. T., Lu, C. L., Lin, H. I., Chen, B. F., & Jow, G. M. (2016). β-elemonic acid inhibits the cell proliferation of human lung adenocarcinoma A549 cells: The role of MAPK, ROS activation and glutathione depletion. Oncology Reports, 35(1), 227-234.